BIOCHEMISTRY
including biophysical chemistry & molecular biology

Article

pubs.acs.org/biochemistry

Mechanism of Amyloid-β Fibril Elongation

Thomas Gurry[†] and Collin M. Stultz*[,†,‡]

[†]Computational and Systems Biology Initiative and Research Laboratory of Electronics, Massachusetts Institute of Technology, Cambridge, Massachusetts 02139-4307, United States

[‡]Department of Electrical Engineering and Computer Science, Institute for Medical Engineering and Sciences, Massachusetts Institute of Technology, Cambridge, Massachusetts 02139-4307, United States

Supporting Information

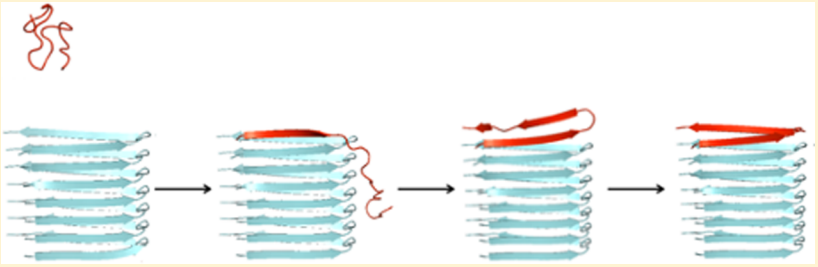

ABSTRACT: Amyloid-β is an intrinsically disordered protein that forms fibrils in the brains of patients with Alzheimer's disease. To explore factors that affect the process of fibril growth, we computed the free energy associated with disordered amyloid-β monomers being added to growing amyloid fibrils using extensive molecular dynamics simulations coupled with umbrella sampling. We find that the mechanisms of Aβ40 and Aβ42 fibril elongation have many features in common, including the formation of an obligate on-pathway β-hairpin intermediate that hydrogen bonds to the fibril core. In addition, our data lead to new hypotheses for how fibrils may serve as secondary nucleation sites that can catalyze the formation of soluble oligomers, a finding in agreement with recent experimental observations. These data provide a detailed mechanistic description of amyloid-β fibril elongation and a structural link between the disordered free monomer and the growth of amyloid fibrils and soluble oligomers.

The amyloid-β (Aβ) protein, a 39−42-residue intrinsically disordered peptide,[1] has long been implicated in the etiology of Alzheimer's disease.[2] It is formed through directed proteolytic cleavage of the amyloid precursor protein by β- and γ-secretase enzymes.[3] Aβ42, the 42-residue cleavage product, has been identified as the most prone to forming aggregates, in the form of both low-molecular weight soluble oligomers and insoluble amyloid fibrils.[4−7] While it is most conspicuously deposited in extracellular plaques composed of amyloid fibrils, a growing body of evidence suggests that soluble oligomeric aggregates, rather than fibrillar aggregates, are responsible for the neurotoxicity observed in Alzheimer's disease, leading to a shift in focus away from the latter and toward the former in the effort to combat the disease.[3,8] Recently, however, the fact that the rate of formation of these oligomeric species of Aβ42 is dependent on the concentration of not only available monomeric Aβ but also amyloid fibrils has come to light, suggesting that fibrils act as catalysts for the formation of toxic oligomeric aggregates,[9] and reinstating the fibrillar species as a protagonist in the disease process.

The mechanistic details of the interplay among monomers, toxic oligomers, and insoluble fibrils remain unknown. Some studies have suggested the existence of a common pathway in which oligomers are on-pathway intermediates in fibril formation, while others propose that oligomers and fibrils are generated through independent pathways.[10] It is likely that therapeutic strategies aimed at stopping the formation of fibrils, which exhibit a degree of polymorphism lower than those of the oligomeric states, will be more tractable in the short to medium term.[11] As such, it is of interest to map out the process of undergoing the transition from a disordered monomer of Aβ to a folded amyloid fibril to identify key intermediates along the pathway that could form viable therapeutic targets. In this article, we present a detailed computational analysis of Aβ42 and Aβ40 fibril elongation using atomistic simulations. In so doing, we recover several independent experimental observations, integrating them into a common pathway, and ascribe a critical role to a β-hairpin intermediate in the process of fibril elongation. Furthermore, we find parallels between the process of amyloid fibril elongation in the context of a disordered protein and the process of globular protein folding in general.

MATERIALS AND METHODS

Model System. For the Aβ42 fibrils, the structure of Protein Data Bank (PDB) entry 2BEG was used as a starting point.[12,13] The structure contains five monomers and was extended to eight

Received: June 5, 2014
Revised: September 6, 2014
Published: October 20, 2014

   dx.doi.org/10.1021/bi500695g | *Biochemistry* 2014, 53, 6981−6991

total monomers in the same configuration (by extending the even end of the fibril) to separate the two ends of the fibril by a greater distance. For the Aβ40 fibrils, structures for the 2-fold positive- and negative-stagger fibrils (PDB entries 2LMN and 2LMO) were used as starting points.[14] Molecular dynamics simulations were performed using a polar hydrogen model.[15] Atoms within the fibril core are fixed, while atoms in the free monomer were allowed to move.

Reaction Coordinates and Umbrella Sampling. The ξ reaction coordinate was computed as the mean of the heavy-atom (N−O) distances between the atoms involved in the intermolecular hydrogen bonds of the Aβ42[12] and Aβ40[14] fibril models (Figure S1 of the Supporting Information). We compute f_β according to the continuous function developed by Vitalis et al.,[16] $f_\beta(\phi_1, \psi_1, \phi_2, \psi_2, ..., \phi_N, \psi_N) = (1/N)\sum_{i=1}^{N} f_\beta^{(i)}(\phi_i, \psi_i)$, where N = 24 for Aβ42 and N = 30 for Aβ40, corresponding to the number of residues in the system that have both φ and ψ angles (the first and last residues have undefined φ and ψ angles, respectively), and

$$f_\beta^{(i)}(\phi_i, \psi_i) = \begin{cases} 1 \text{ if } (\phi_i - \phi_\beta)^2 + (\psi_i - \psi_\beta)^2 < r_\beta^2 \\ \exp\left[-\tau_\beta D_{(i)}^2\right] \text{ otherwise} \end{cases} \quad (1)$$

where $(\varphi_\beta, \psi_\beta)$ is the center of a circular region in Ramachandran space with radius r_β, $D_{(i)}^2 = \{[(\phi_i - \phi_\beta)^2 + (\psi_i - \psi_\beta)^2]^{1/2} - r_\beta\}^2$ [the square Euclidean distance between (φ_i, ψ_i) and the boundary of the basin], and τ_β is a decay constant. Because differences between angles can take two possible values due to their periodic nature, any distance in Ramachandran space, including $D_{(i)}^2$ and angle differences, e.g., $\phi_i - \phi_\beta$, is interpreted as the minimal possible distance in this space. The center of the basin $(\varphi_\beta, \psi_\beta)$ was defined by $\varphi_\beta = -152.00°$ and $\psi_\beta = 142.00°$, i.e., the values used by Vitalis et al.[16]

The parameters τ_β and r_β were chosen to optimize agreement with strand assignments made by DSSP.[17] More precisely, for a given structure in the PDB, one can calculate f_β, which corresponds to the fraction of residues that adopt extended structure consistent with a β-strand, and one can compute the β-strand percentage using DSSP. The parameters τ_β and r_β were chosen to ensure that these calculated values would be similar for a relatively large set of structures chosen from the PDB. Only structures consisting of a single chain (with no ligands) were used. Moreover, we ensured that any two structures in the final set had <30% identical sequences. This resulted in 5827 structures. A grid search was performed for values of τ_β between 0.0001 and 0.04 deg^{-2} in increments of 0.0001 deg^{-2}, and for values of r_β between 20° and 100° in increments of 1°.

In practice, agreement with the DSSP strand content values was achieved by minimizing the objective function $f_{obj} = k_1(1/\rho) + k_2|m - 1|$, where ρ is the correlation between the f_β and DSSP scores, m is the gradient of the linear regression of f_β against the DSSP-E score, and k_1 and k_2 are normalizing constants to ensure that the correlation term $(1/\rho)$ and the gradient term $(m - 1)$ have similar ranges over the data set. Minimizing this function yielded the following final parameters: τ_β = 0.0029 deg^{-2}, and r_β = 62°. With these values, we obtained a correlation of 0.93 between f_β and the DSSP scores, and the corresponding linear regression had a gradient of 0.96.

The final potential energy function is of the form $U_{umbrella} = U_{CHARMM} + U_\xi + U_{f_\beta}$, where $U_\xi = k_\xi(\xi - \xi_0)^2$, $U_{f_\beta} = k_{f_\beta}(f_\beta - f_0)^2$ (defining a sampling window centered about ξ_0 and f_0), and U_{CHARMM} is the CHARMM potential energy function.[18] To use this function for dynamical simulations, the U_{f_β} potential (along with its derivative, which is needed for the force calculations) needs to be added to the CHARMM code. However, while one can use the form of eq 1 for dynamical simulations, this is not optimal because it is not continuous at the basin boundary, r_β. This leads to unstable trajectories. Consequently, we also developed an alternate form for $f_\beta^{(i)}(\phi_i, \psi_i)$ based on a continuous, two-dimensional Gaussian function for f_β:

$$f_\beta^{(i)}(\phi_i, \psi_i) = \exp\left\{-\left[\frac{(\phi_i - \phi_0)^2 + (\psi_i - \psi_0)^2}{2\sigma^2}\right]\right\} \quad (2)$$

The center and standard deviation of this alternate form were chosen to again match those calculated with DSSP (as outlined above). Preliminary data suggest that both methods yield similar results, while the latter method had greater numerical stability.

The harmonic force constants k_{f_β} and k_ξ were chosen to obtain adequate overlap between histograms arising from adjacent umbrella sampling windows. Sampling was initiated from reaction coordinate values closest to the fibril model configuration. In the Aβ42 model, this corresponds to an f_β value of 0.75 and a ξ value of 2.73 Å, i.e., f_β = 10/13 and ξ = 3 Å. f_β was sampled with values of f_0 between 0 and 1 in increments of 1/13 (∼0.08) for the Aβ42 fibril, which roughly translates into biasing the monomer along its strand contents two residues at a time, while for the Aβ40 fibrils, increments of 1/6 (∼0.17) were used. ξ was sampled between ξ_0 values of 3 and 70 Å in both cases. Increments of ξ_0 were spaced by 0.5 Å for 3 Å ≤ ξ_0 < 17 Å, and the spacing increased to 1 Å for 17 Å ≤ ξ_0 ≤ 42 Å and to 2 Å onward until ξ_0 = 70 Å for Aβ42. The Aβ0 increments of ξ_0 were spaced by 0.5 Å for 3 Å ≤ ξ_0 < 10 Å, and the spacing increased to 1 Å thereafter. k_{f_β} was fixed at 350 kcal mol^{-1}. k_ξ was set to 1 kcal mol^{-1} Å^{-2} for 3 Å ≤ ξ_0 < 42 Å and to 0.01 kcal mol^{-1} Å^{-2} for 42 Å ≤ ξ_0 ≤ 70 Å. Initial data suggested that in certain regions, sampling was insufficient in the ξ reaction coordinate. In those cases, additional sampling was performed at additional values of ξ (Figure S7 of the Supporting Information).

The umbrella potential for the ξ reaction coordinate was included by using the RESD (REStrained Distances) command in the CHARMM molecular dynamics package (version 36b2).[18] For each pair of values (f_0, ξ_0) (i.e., a "window"), the system was equilibrated for 5 ns followed by a 45 ns production run (Figures S8 and S9 of the Supporting Information). All simulations utilized an implicit model for solvent. While simulations with explicit solvent may provide a more realistic representation of the solvent environment, they result in lengthy production runs for achieving convergence because relaxation of explicit water at each value of the reaction coordinate can be very long. For this reason, most umbrella sampling simulations with explicit solvent have been applied to systems that are considerably smaller than that considered in this study or have utilized a one-dimensional reaction coordinate.[19−21] To reach the simulation time scales needed to ensure convergence of the reaction coordinates in our umbrella sampling windows, we conducted these simulations using the implicit solvent model EEF1[22] because (1) prior work suggests that one can obtain free energy profiles (for peptides that form aggregates) with this model that are similar to those that would be obtained with explicit solvent[23] and (2) other studies that looked at dimerization of peptides that form amyloid precursors suggest that EEF1 produces results that are the closest to experiment (relative to generalized Born and analytic continuum electrostatic models).[24]

dx.doi.org/10.1021/bi500695g | Biochemistry 2014, 53, 6981−6991

The initial systems were linearly heated to 310 K over 100 ps and then coupled to a Nosé−Hoover thermostat at the same temperature.[25] Bond lengths involving hydrogens were fixed using SHAKE, and simulations were performed using CHARMM version 36b2 with a 2 fs time step.[18] The total simulation time for the Aβ40 and Aβ42 models was ∼100 μs. Values of the reaction coordinates from the trajectories were saved every 5 ps, yielding 9000 data points each per window. The resulting biased probability distributions were recombined to generate the final unbiased PMF using Grossfield's standard implementation of the two-dimensional weighted histogram analysis method (2D-WHAM).[26,27]

In addition to the potential of mean force calculations outlined above, we performed unrestrained simulations for both Aβ40 and Aβ42 models. In each case, the setups were identical to the umbrella sampling simulations, except that the systems were linearly heated to 450 K, also over 100 ps, after which production runs of 1 μs were performed, and no biasing potentials were employed.

RESULTS

Our calculations began with a model of the Aβ(17−42) fibril core that was constructed using constraints arising from different experimental observations [e.g., hydrogen/deuterium exchange, mutagenesis studies, and solid-state nuclear magnetic resonance (NMR)] (PDB entry 2BEG).[12,13] This structure is composed of two intermolecular, in-register β-sheets formed by residues 18−26 (strand β1) and 31−42 (strand β2), with the first 16 N-terminal residues being disordered and external to the fibril.[12] To study the process of fibril elongation, we began with this model that we term the "fibril core" (consisting of residues 17−42) and calculated the free energy for the folding of an Aβ monomer being added to the odd end of the fibril core (Figure 1A). In practice, the free energy calculations begin with the folded state (i.e., with the Aβ42 monomer already bound to the fibril core) and the free energy profile for unbinding (or unfolding) of an Aβ42 monomer is calculated, thereby allowing the simulations to begin with a well-defined structure. Because the free energy itself is a state function, the final free energy surface, in principle, is not determined by the order in which the calculations proceed.

The free energy associated with folding was calculated as a function of two reaction coordinates: the average heavy-atom (N−O) distance between pairs of atoms that form intermolecular hydrogen bonds between the Aβ monomer and the strands at the odd end of the fibril core, ξ, and the fraction of residues in the Aβ monomer adopting β-strand secondary structure, f_β. The former acts as a proxy for measuring the distance from the Aβ monomer to the fibril (Figure 1B), and the latter ensures that we sample a wide range of β-strand content as the monomeric disordered protein folds to the fibrillar state (Figure 1C).[28] The resulting free energy surface (FES) is a function of these two reaction coordinates and is also termed a potential of mean force.[29]

To construct a free energy surface, we use umbrella sampling with implicit solvent. The approach requires that we generate continuous "umbrella" potentials to ensure that a wide range of values for the reaction coordinates are sampled.[29] A simple harmonic function is used to restrain the average N−O distance to any desired value. To construct a continuous function that would restrain the fraction of residues that would be in a β-strand conformation, f_β, we used a previously developed formalism that defines a β-basin in dihedral angle space[16] (cf. Materials and Methods). Once this function is specified, a simple harmonic

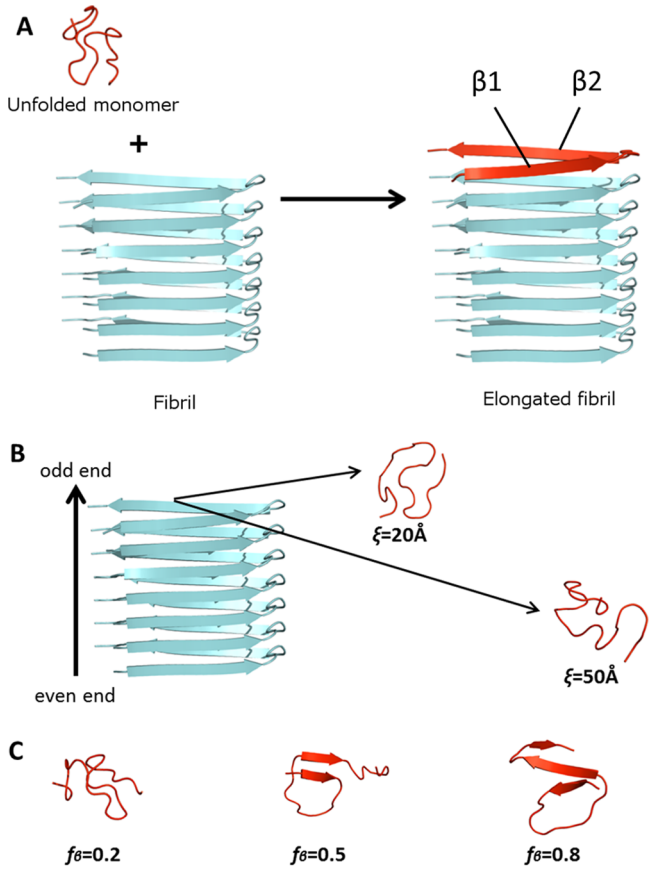

Figure 1. Schematic of the elongation reaction and the reaction coordinates used. The backbone trace of the Aβ monomer is colored red, while the backbone trace of the "fibril core" is colored cyan. Strands in the bound state (A) are labeled as β1 (N-terminal) and β2 (C-terminal). Different values of ξ and f_β are shown to illustrate the reaction coordinate and the even and odd ends of the fibril core (B and C, respectively).

function can also be applied to restrain the system to any particular β-strand content. By restraining the simulation to specified values of ξ and f_β, we can ensure that a wide range of conformational space is sampled. Moreover, while sampling is employed on a biased energy surface, the final calculated free energy is independent of the choice of the umbrella potentials chosen and therefore represents the true free energy profile calculated from an unbiased energy surface.[27,29]

The resulting free energy surface has a broad global energy minimum corresponding to the bound, fibrillar state, F (Figure 2). From these data, we identify the minimum free energy path from the unbound state to the bound, folded state (centered about ξ = 3 Å), i.e., the path that minimizes the work associated with moving from one state to the other (Figure 2). We can also identify paths that are within 3kT of the lowest-energy path, thereby providing information about the diversity of states that are sampled as the system proceeds from the unfolded to the folded state.

Low-energy paths connecting the unfolded state to the final folded state have many features in common. To illustrate this, we can identify six states that are sampled along the lowest-energy path and corresponding structures that are at least 3kT from these states (points a−c, H, T*, and F in Figure 2). As the monomer approaches the fibril core, it preferentially makes contacts with residues 25−31 in the fibril that form turns

dx.doi.org/10.1021/bi500695g | Biochemistry 2014, 53, 6981−6991

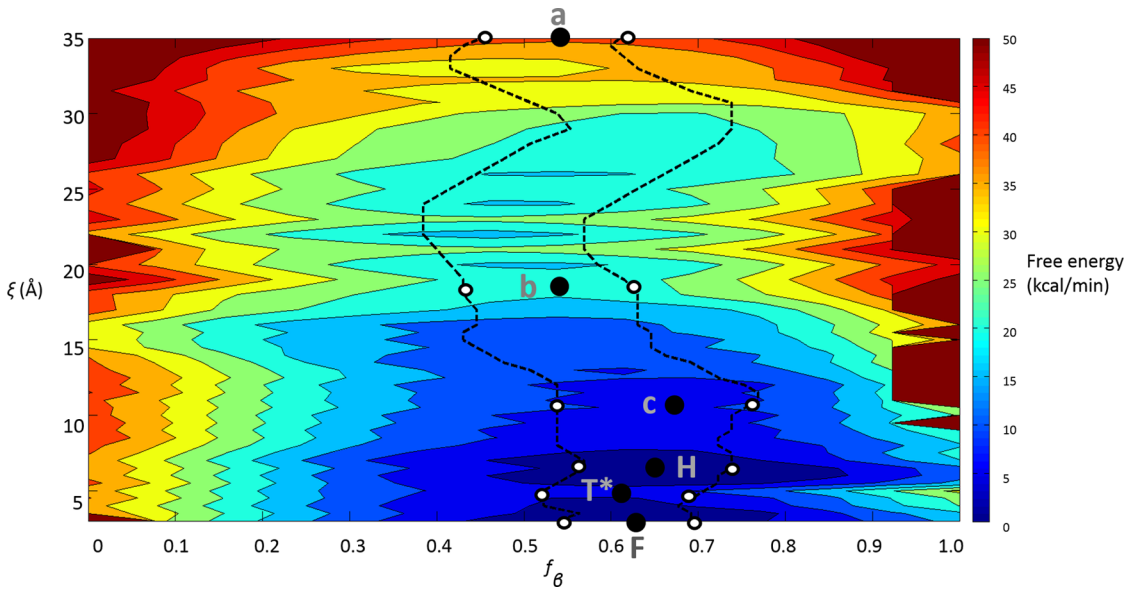

Figure 2. Contour plot of the free energy surface of monomeric Aβ(17−42) as a function of the proximity to the fibril-bound state (ξ) and β-strand content (f_β), shown for ξ values of <35 Å. Points a−c, H, T*, and F along the minimum energy path between the unbound and bound states are explicitly shown. Dotted black lines represent a 3kT envelope around the minimum energy path. Only free energies of states that have an average N−O distance between the Aβ monomer and the fibril core of <35 Å are shown. The full PMF can be found in the Supporting Information.

between the strands (Figure 3, state a). Essentially, the monomer "rolls" along the fibril making nonspecific interactions between the monomer and exposed side chain of Asn 27, as well as the backbone carbonyl of Lys 28 and backbone nitrogen of Ala 30 (Figure S3 of the Supporting Information). Association with the odd end of the fibril then ensues, followed by the formation of a strand (β1) at the odd end (Figure 3, state b) with the release of roughly 15 kcal/mol (Figure 2). While the β1 strand [residues 18−26 (Figure S1 of the Supporting Information)] of the monomer remains bound at the odd end, the C-terminal residues sample a range of distinct conformations, some of which continue to make contact with the turn residues in the fibril core. Progressive formation of intramolecular hydrogen bonds eventually leads to the formation of structures that contain a β-hairpin (Figure 3, states c and H). Interestingly, structure c contains turns at residues found to be solvent-exposed in amide exchange NMR experiments performed on Aβ42 oligomers and closely resembles the proposed structure in that same study, highlighting the possibility that soluble oligomers and fibrils share common intermediates for their formation.[30] To reach the final folded state from H, a free energy barrier of approximately 4 kcal/mol has to be overcome. In the associated transition state T*, intramolecular hydrogen bonds between strands β1 and β2 in the hairpin are broken (Figures 3 and 4). In the final state, these intramolecular interactions are replaced with intermolecular hydrogen bonds between the Aβ monomer and the fibril core (Figure 4).

To explore how our findings depend on the choice of starting structure, and Aβ sequence, we recomputed free energy surfaces using a different structure for the fibril core. Because a number of fibril structures in the structural database are composed of two or more filaments,[14,31,32] we chose two structural models of Aβ40 fibers that were built using experimental constraints arising from solid-state NMR experiments. While both structures consist of residues 9−40 as the eight N-terminal residues were disordered and contain two filaments, they differ with respect to the relative positions and orientations of the β-sheets (PDB entries 2LMN and 2LMO, respectively).[13,14] In particular, the restraints used to construct these fibril structures were compatible with both positive- and negative-stagger models, and therefore, two models could be built from the data.[14] However, recent computational studies of models of Aβ40 fibrils suggest that only the negative stagger can form left-handed helical superstructures, the twist that has been observed in scanning electron microscopy studies of amyloid superstructures.[33,34] Indeed, our own data are consistent with these observations as we find that the global free energy minimum for the Aβ40 structure with positive stagger is not the fibrillar state (cf. Figures S4 and S5 of the Supporting Information).

The free energy surface for the negative-stagger, 2-fold-symmetric Aβ40 fibril has a broad global energy minimum corresponding to the bound, fibrillar state (Figure 5). As described above, we identified the minimum free energy path from the unbound state to the bound, folded state (centered about ξ = 3.5 Å) (Figure 5), along with paths that are at least 3kT from the minimum energy path.

Low-energy paths from the unbound state to the bound, folded state share many features with one another. The incoming monomer initially interacts with the second filament of the fibril (state a, Figures 5 and 6). The N-terminal β1 strand then associates with the odd end of the first filament (state b, Figures 5 and 6). Next, strand β2 forms intramolecular hydrogen bonds with strand β1, forming a hairpin intermediate, H (Figure 6, state H). The reaction then proceeds through several states in which the intramolecular β1−β2 hydrogen bonds break and are replaced with intermolecular hydrogen bonds between adjacent β2 strands at the odd end of the fibril, ending in the fibrillar conformation, F (Figure 7).

Calculating a free energy surface requires one to prespecify a set of reaction coordinates. While the calculated free energy difference between the unbound and bound (folded) state is independent of the path, the intermediates sampled along the path will depend on the choice of the reaction coordinates. To test whether the observed intermediates are artifacts of the choice of reaction coordinates, we performed unbiased unfolding simulations of the Aβ(17−42) and Aβ(9−40) fibril core models.

dx.doi.org/10.1021/bi500695g | *Biochemistry* 2014, 53, 6981−6991

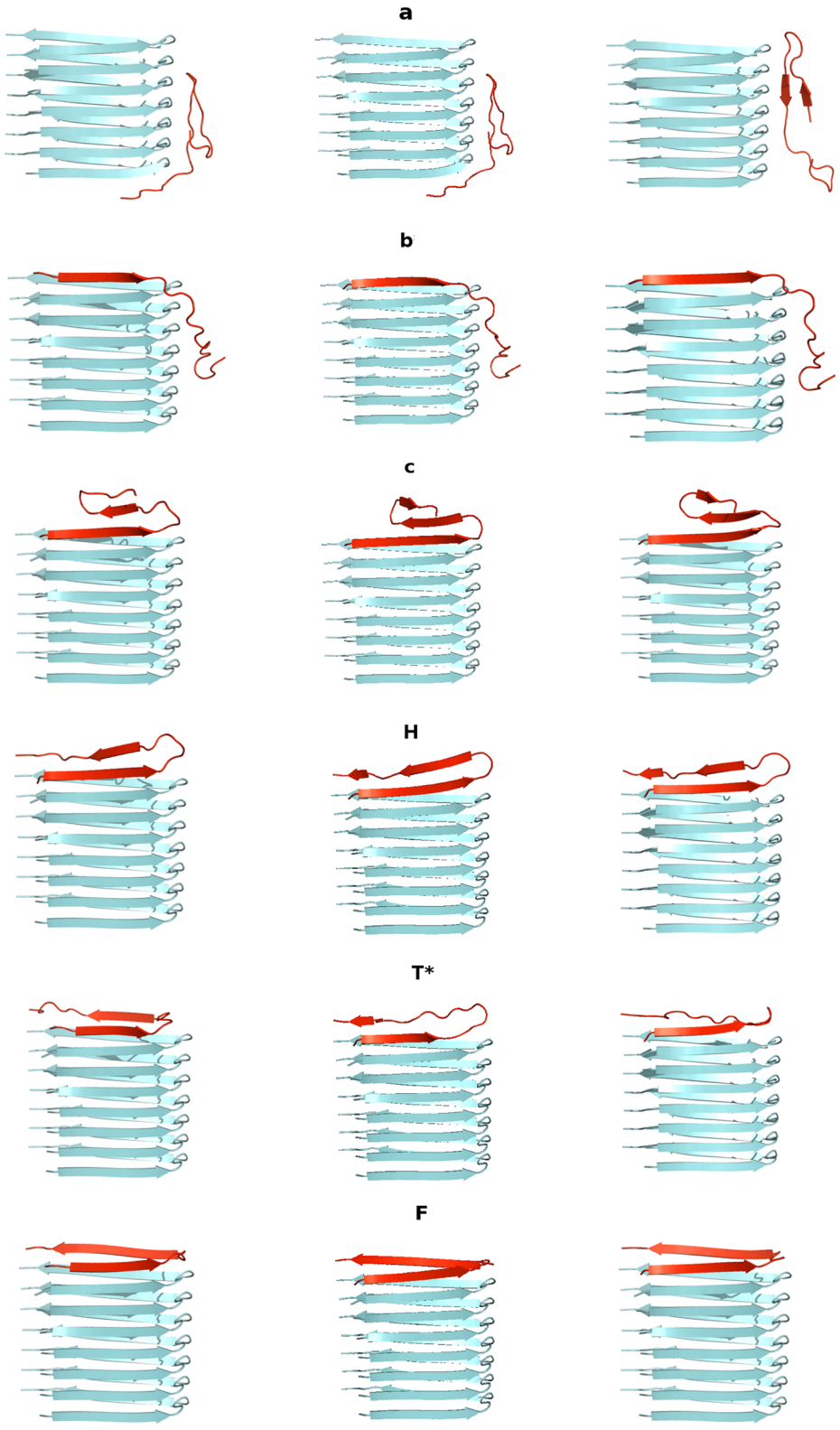

Figure 3. Structures for states a−c, H, T*, and F. The middle structures are on the lowest-energy path, and flanking structures have free energies that are at least $3kT$ higher.

Although these simulations do not allow us to calculate precise free energy differences between states (as opposed to the detailed free energy simulations described above), they do allow us to probe the dynamics of unrestrained monomers as they unbind, without any bias introduced by a prespecified choice of reaction coordinate.

We performed a 1 μs unbiased simulation at 450 K on the same Aβ(17−42) fibril core used in the umbrella sampling simulations, again with the EEF1 implicit solvent model. Over the course of the unfolding simulation, we observe a transition from the fibrillar state, F, to a hairpin state, H, in which strands β1 and β2 form intramolecular hydrogen bonds, which are then broken

dx.doi.org/10.1021/bi500695g | *Biochemistry* 2014, 53, 6981−6991

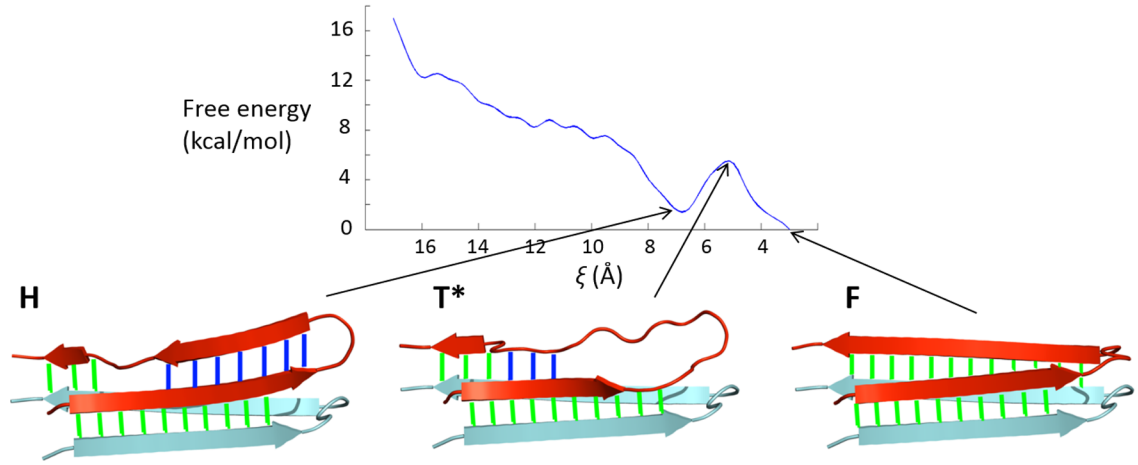

Figure 4. Transition from a hairpin structure (H) through the transition state (T*) to the fibrillar state (F). The minimum free energy path as a function of ξ for ξ values of <17 Å is shown. Intermolecular hydrogen bonds are colored green, while intramolecular hydrogen bonds are colored dark blue. In hairpin state H, strand β1 (residues 18−26) forms the intermolecular hydrogen bonds with the adjacent strand in the fibril core while strand β2 (residues 31−41) forms intramolecular hydrogen bonds with strand β1. In transition state T*, most of the intramolecular hydrogen bonds between strands β1 and β2 are broken and intermolecular hydrogen bonds between strand β2 and the fibril core form. In bound state F, all hydrogen bonds are intermolecular.

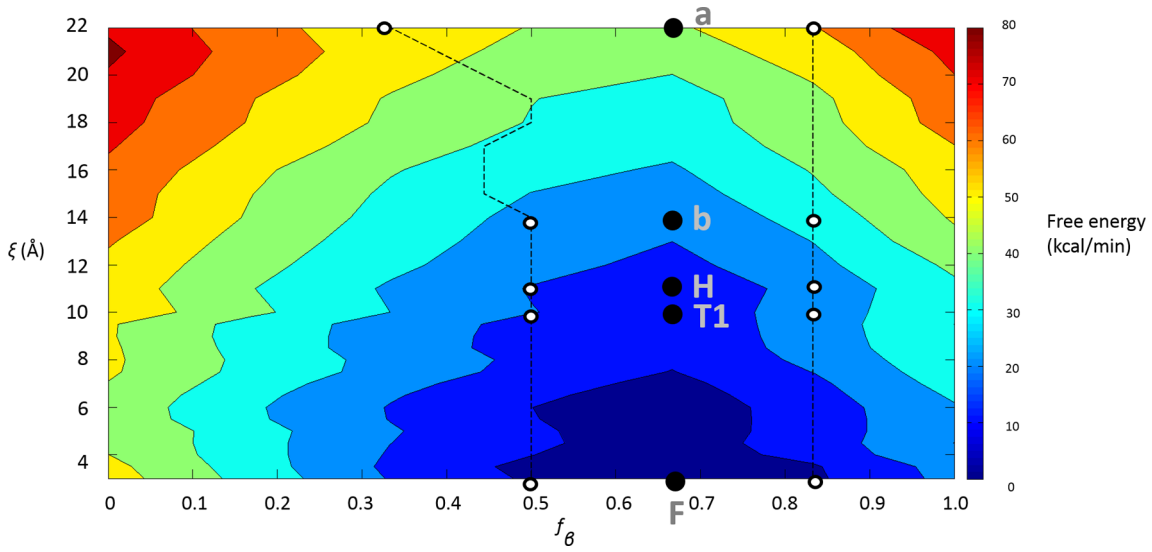

Figure 5. Contour plot of the PMF for the folding of Aβ(9−40) as a function of the proximity to the fibril-bound state (ξ) and β-strand content (f_β), shown for ξ values of <22 Å. Points a, b, H, T1, and F along the minimum energy path between the unbound and bound states are explicitly shown. Dotted black lines represent states that are at least 3kT from the lowest-energy path. Only free energies of states that have an average N−O distance between the Aβ monomer and the fibril core of <22 Å are shown. The full PMF can be found in the Supporting Information.

upon returning to the fibrillar state (Figure 8). This is consistent with an intermediate, hairpin state H that is less stable than F but is within thermal reach of F, observations in agreement with the lowest-energy path on our free energy surface (Figure 4). Similar unbiased simulations at 450 K of the Aβ(9−40) fibril core were performed, again using the EEF1 implicit solvent model. Conformations sampled during the simulation are consistent with those derived from the free energy surfaces (Figure 9). More specifically, the trajectory proceeds from fibrillar state F by breaking the intermolecular hydrogen bonds of strand β2 via states T1 and I1, followed by association of strand β2 with the second filament of the fibril structure (state b) and subsequent dissociation, data that are in good agreement with states observed on the calculated free energy surface (Figure 7). We note that no hairpin state was significantly sampled during the course of our Aβ40 simulations, a finding consistent with the observation that this state has a relatively high energy on the free energy surface.

DISCUSSION

Aβ aggregation lies at the heart of Alzheimer's disease pathology, in the form of amyloid fibrils and lower-molecular weight soluble oligomers. Through extensive umbrella sampling simulations performed on experimentally derived models of fibril structures, we compute a free energy surface for the process of Aβ42 and Aβ40 fibril elongation. We find that fibril elongation occurs on downhill free energy pathways, ending in the fibrillar conformation, F, which corresponds to the global minimum on the free energy surfaces of both Aβ42 and negative-stagger Aβ40 fibrils, but not in positive-stagger Aβ40 fibrils. The inability of the positive-stagger Aβ40 fibril to elongate is consistent with prior data that suggest that positive-stagger filaments cannot adopt the superstructural helical twist that has been observed in scanning electron microscopic studies of amyloid fibrils; i.e., positive-

dx.doi.org/10.1021/bi500695g | *Biochemistry* 2014, 53, 6981−6991

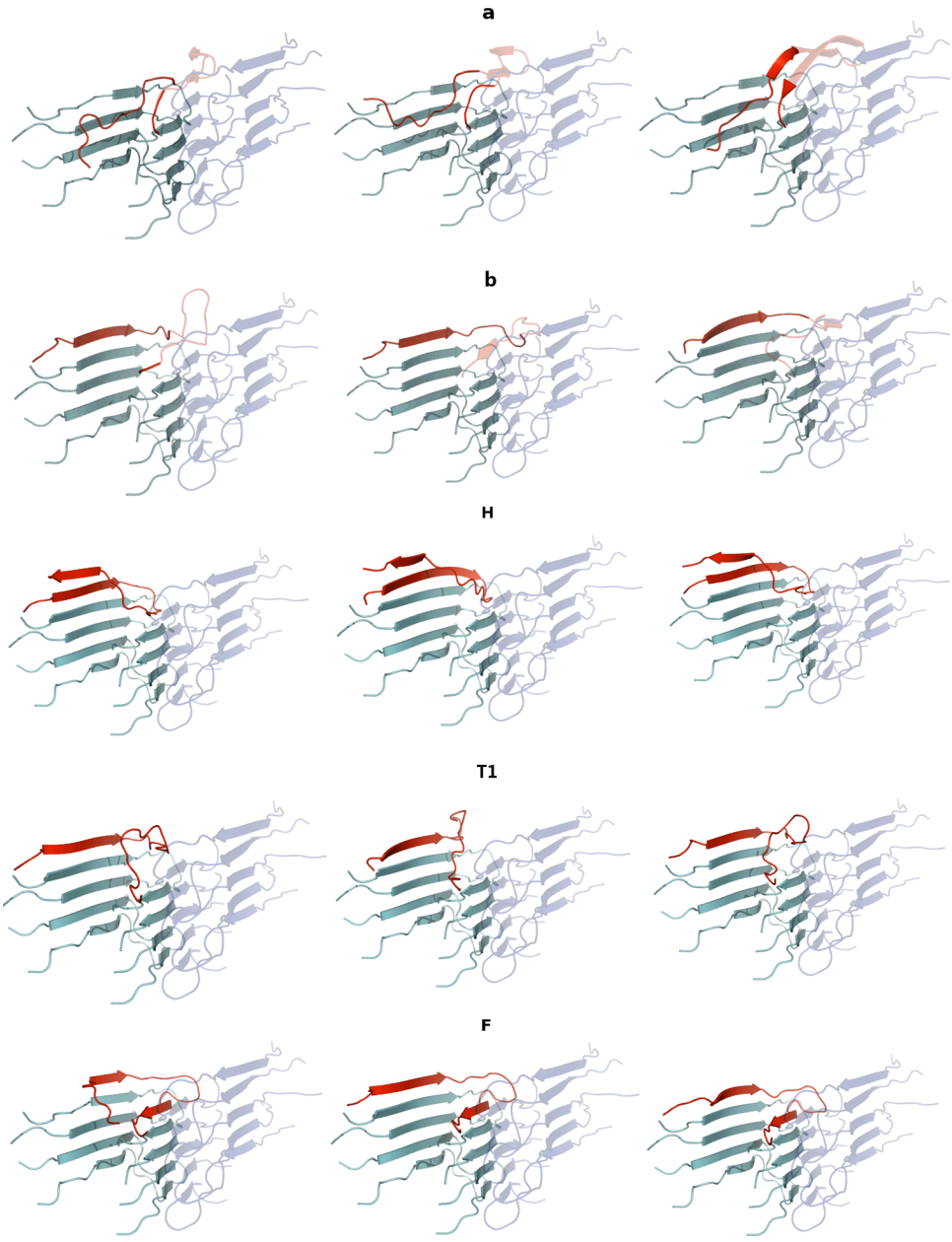

Figure 6. Structures for intermediate states a, b, H, T1, and F. The AB40 structure is composed of two filaments. The first filament is colored cyan, and the second is shown in transparent blue. Regions of the incoming monomer (red) that are associated with the second filament are transparent, as well. The middle structures are on the lowest-energy path and flanking higher-energy structures having free energies that are at least 3 kcal/mol higher.

stagger protofibrils would not grow to form mature fibrils with the correct helical twist.[33,34]

Our results for both Aβ42 and Aβ40 suggest features that are common to the elongation process for both proteins. (1) The monomer associates with the odd end of the fibril by forming an N-terminal β1 strand that forms intermolecular hydrogen bonds with the fibril core. (2) Association with the odd end of the fibril is followed by the formation of a common intermediate, H, which takes the form of a β-hairpin in which strand β1 forms intermolecular hydrogen bonds to the fibril core and strand β2 forms intramolecular hydrogen bonds with strand β1. (3) Disruption of the intramolecular hydrogen bonds within the hairpin leads to formation of the final bound state in which the monomer forms only intermolecular hydrogen bonds with the fibril core. For both sequences, a β-hairpin is an obligate intermediate on the folding pathway. These data are consistent with the observation that sequestration of a β-hairpin conformation of Aβ40 slows aggregation.[35] Additionally, stabilizing the bend between the two β-strands leads to a significant increase in the rate of fibrillogenesis, a finding that also is consistent with our results.[36]

Several studies suggest that aggregation-prone states are sparsely populated in the absence of fibril cores and that stabilization of these states leads to an increase in the rate of fibril formation.[36−38] Indeed, in a previous study, we generated structural ensembles for Aβ42 and Aβ40, in the absence of a fibril core, using a number of experimental observables as a guide, and observed that β-hairpin conformations were infrequently sampled for both Aβ42 and Aβ40.[39] Although these states are not highly populated, an analysis of the ensembles suggests that Aβ42 is approximately 10 times more likely than Aβ40 to adopt β-hairpin structures. Taken together, these data help to explain

dx.doi.org/10.1021/bi500695g | *Biochemistry* 2014, 53, 6981−6991

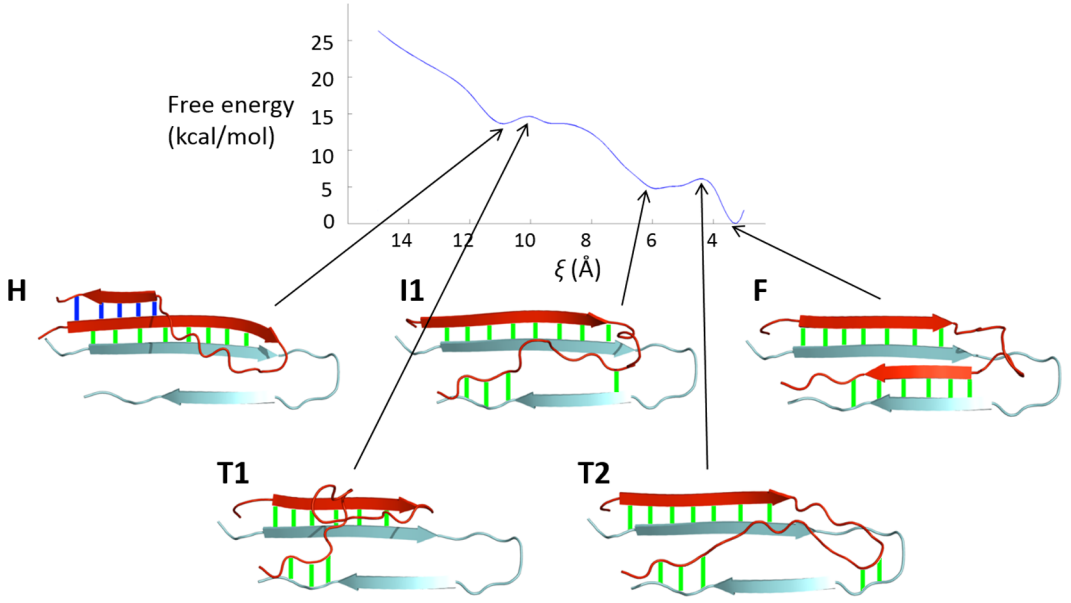

Figure 7. Transition from the hairpin structure (H) through the transition states (T1 and T2) to the fibrillar state (F). The minimum free energy path as a function of ξ for ξ values of <15 Å is shown. Intermolecular hydrogen bonds are colored green, while intramolecular hydrogen bonds are colored dark blue.

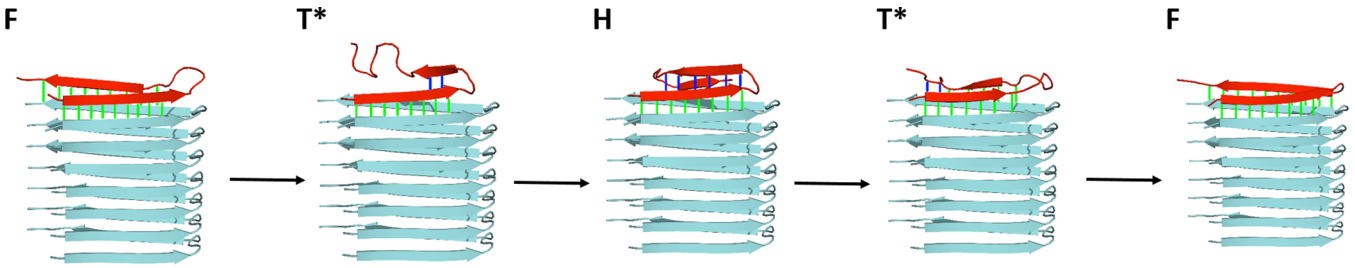

Figure 8. Structures sampled during the 1 μs unfolding simulation at 450 K of the Aβ(17−42) fibril core. The states are presented in chronological order and were sampled at 500, 550, 600, 700, and 850 ns.

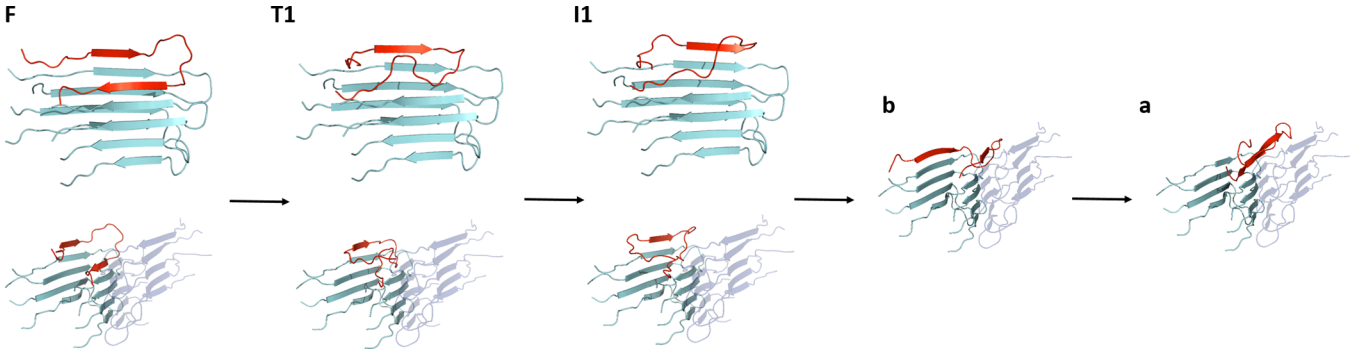

Figure 9. Structures sampled during the 1 μs unfolding simulation at 450 K of the Aβ(9−40) fibril core. The states are presented in chronological order and were sampled at 0, 50, 125, 350, and 550 ns.

why Aβ42 forms fibrils much faster than Aβ40; i.e., Aβ42 is more likely to populate intermediates along the folding pathway. This observation becomes even more pronounced in the presence of the fibril core. When the fibril is present, β-hairpin structures for Aβ42 have energies that are only a few kT higher than that of the native, folded state while β-hairpin structures Aβ40 have energies that are significantly higher than the native-state energy (Figures 4 and 7). These data highlight at least one mechanism whereby the presence of fibrils can accelerate fibrillogenesis. More precisely, when fibrils are present, some Aβ isoforms may be more likely to adopt aggregation-prone structures that can be incorporated into a growing fibril.

A number of studies have attempted to isolate key molecular features involved in fibril or oligomer growth of Aβ40 or smaller amyloidogenic peptides derived from the Aβ40 sequence.[40−42] A common feature that arises from these studies is that addition of a monomer to a β-rich template representing either a soluble oligomer or a protofibril occurs via a "dock-lock" mechanism that is similar to the scheme originally proposed by Esler et al.[43] Docking consists of an incoming monomer loosely associating

dx.doi.org/10.1021/bi500695g | *Biochemistry* 2014, 53, 6981−6991

with the template in a manner such that it can readily dissociate. Locking involves the formation of hydrogen bonds to the template, yielding a structure for which monomer dissociation is unlikely. In our studies, the monomer initially interacts with the template via nonspecific interactions (Figures 3 and 6, state a) that can involve regions other than the odd end of the fibril. Locking (a relatively slow process) occurs when strand β1 of the incoming monomer binds to the odd end of the fibril. Subsequent structural rearrangements in the monomer lead to the formation of the final folded structure.

The free energy surfaces were calculated as a function of two reaction coordinates: ξ, the average N−O distance between the free monomer and the odd end of the fibril, and f_β, the fraction of residues that have ϕ and ψ angles that are consistent with a β-strand. Because the addition of a monomer to the odd end of the fibril can be viewed as a ligand binding reaction, during which the ligand changes its structure upon binding, we chose a reaction coordinate, ξ, which quantifies the distance from the monomer to the fibril core, and that ensures that the monomer samples states that have the correct hydrogen bonding pattern. The second reaction coordinate, f_β, which quantifies the β-strand content of the incoming monomer, ensures that we sample a variety of β-strand content at any given distance from the fibril core. Indeed, similar reaction coordinates have been used to study ligand binding and protein association.[23,44−46] Nevertheless, it is important to note that while the calculated free energy difference between the unbound and bound (or folded) states is a function of state, and therefore independent of the path chosen to go from the unbound to the bound state, the observed intermediates are dependent on the choice of reaction coordinates. Although the relatively lengthy simulation time for these calculations (~100 μs total for both the Aβ40 and Aβ42 models) allows the system to sample a variety of different structures during the umbrella sampling runs (e.g., Figure S10a,b of the Supporting Information), the choice of the reaction coordinates will influence the structures sampled on the lowest-energy path.

Ideally, one could gain insight into the folding pathway from unbiased simulations starting from the unfolded (unbound) state under conditions where the folded state is stable. Because folding occurs on time scales that are typically beyond the reach of atomistic simulations, such simulations are typically not tractable. Information about the folding pathway can sometimes be garnered from unfolding simulations, where folded protein structures are subjected to conditions where the unfolded state is the most stable, e.g., simulations at high temperatures. While it is clear that unfolding at high temperatures is different from folding (which occurs at lower temperatures), a number of studies suggest that high-temperature unfolding simulations can capture qualitative aspects of the folding process.[47,48] In this regard, we note that unbiased high-temperature unfolding simulations of the Aβ42 and Aβ40 fibril core models sample structures that are similar to those sampled on low-energy paths from the calculated free energy surfaces (Figures 4 and 8 and Figures 7 and 9). The fact that the unfolding simulations yield observations that are similar to those arising from the lowest-energy paths, on the calculated free energy surfaces, argues that the lowest-free energy paths are not simply an artifact of the chosen reaction coordinates. Nevertheless, to further assess the significance of these observations, it is important to compare observations arising from the lowest-energy path to known experimental observables.

In a recent study, Fawzi et al. performed dark-state exchange saturation transfer (DEST) experiments on Aβ protofibrils, providing new insights into the dynamics of monomeric Aβ on the surface of protofibrils.[49] While these data suggest that residues in strands β1 and β2 are essentially equally likely to make direct contacts with the protofibril, measured ^{15}N transverse relaxation rates argue that residues in strand β1 of Aβ40 are less flexible than residues in strand β2. Our findings are consistent with these observations in that we find that Aβ40 binds to the odd end of the fibril through its β1 strand while residues in the β2 strand remain unstructured and make nonspecific contacts with the fibril core (Figure 6, state b). Indeed, preferential association of the N-termini of an incoming Aβ peptide was observed in another work examining the energetics of fibril growth.[41] Moreover, a comparison of ^{15}N transverse relaxation rates of Aβ40 and Aβ42 further suggests that residues in strand β2 of Aβ40 are more flexible than residues in strand β2 of Aβ42.[49] Our data are also consistent with these findings because folding pathways for Aβ42 contain hairpin structures that are not present in the Aβ40 folding pathways (Figure 3, state c). In these structures, residues in strand β2 of Aβ42 make a series of intramolecular hydrogen bonds that further limit their flexibility. Lastly, a number of mutations that are known to affect the kinetics of fibril formation have been described. For example, one study found that the Flemish mutant A21G decreases the kinetics of fibril extension relative to that of the wild type, while the Dutch mutant E22Q increases it.[50] Another found that the Arctic mutation E22G increased the rate of protofibril formation.[51] It is interesting to note that these mutations and several others cluster in a region of the Aβ peptide that corresponds to strand β1 of the fibril structures we have studied (Figure S1 of the Supporting Information).[51] Because our data suggest that strand β1 associates first and most stably with the odd end of the fibril, it is likely that mutations that increase or decrease the propensity for strand formation in this region would affect fibrillization kinetics.

While the free energy surfaces for Aβ42 and Aβ40 fibril elongation share common features, there are significant differences between them. The main difference is that the Aβ42 monomer undergoes a phase in which it essentially "rolls" along the fibril, making contacts with fibril residues that form turns in the structure, before attaching to the odd end, while this behavior is not seen in low-energy paths associated with Aβ40 folding. Moreover, the Aβ42 folding pathway involves the formation of an S-shaped hairpin structure (Figure 3, state c), a structure that does not occur in the Aβ40 fiber elongation pathway. Recent experimental data, in the form of kinetic assays, selective radiolabeling, and cell viability experiments, suggest that Aβ42 fibrils catalyze the formation of soluble oligomers through a secondary nucleation pathway.[9] Rolling of Aβ42 monomers on the fibril surface may provide a mechanism for increasing the local concentration of monomeric states. In this sense, the fibril surface, particularly regions that form turns in the fibril structure, may provide a secondary nucleation site that allows monomers to self-associate at a rate higher than the rate that would be allowed in the surrounding solvent.[9] Moreover, the Aβ42 folding pathway involves the formation of an S-shaped structure that has been postulated to exist in Aβ42 oligomers,[30] a process likely facilitated by the two additional hydrophobic C-terminal residues in Aβ42. These data are consistent with the notion that soluble oligomers and fibrils share common intermediates with regard to their formation. Because soluble oligomers can induce fibril

dx.doi.org/10.1021/bi500695g | Biochemistry 2014, 53, 6981−6991

formation, the presence of the fibril can induce additional fibril deposition by catalyzing the formation of soluble oligomers.[52]

While these results are encouraging, it is important to note that some of these differences between the folding pathways of Aβ40 and Aβ42 may be due to the fact that the Aβ40 starting structure has two filaments while the Aβ42 starting structure has one filament (the only available fibril structure for Aβ42 at the time that this study was performed). It is difficult to know how our results could be generalized if these calculations were performed on Aβ42 structures that have multiple filaments. In this vein, we note that after the completion of this work a structural model of Aβ40 fibrils was reported that was derived from seeded fibril growth using brain extracts from a patient with Alzheimer's disease.[53] Because this structure is significantly different from the other fibril structures that have been described in the literature, it is not clear how our findings for Aβ40 could be generalized to these data.

An additional limitation of our study is that the free energy surfaces were computed using an implicit solvent model. Although the solvent model was chosen because it has been shown to yield calculated free energy profiles that are similar to what would be obtained with explicit solvent (at least for some amyloidogenic peptides),[23,24] explicit water molecules may play an important role in the kinetics and thermodynamics of Aβ peptides.[38] Nonetheless, these simulations provide useful insights into the aggregation process and, more importantly, a set of hypotheses that provide fodder for future experiments. For example, our data also suggest that mutations affecting the bend between strands β1 and β2 (residues 23−31) may hinder rolling of incoming monomers and consequently the rate of soluble oligomer formation, but it is unclear how this observation can be generalized to different fibril morphologies and Aβ isoforms. In addition, our results argue that longer fibrils would present a larger surface area on which monomers could self-associate, thereby suggesting that the rate of soluble oligomer formation would be increased in the presence of the larger fibrils.

Overall, the calculated free energy surfaces provide a new testable hypothesis regarding the mechanism of Aβ fibril elongation. Indeed, we argue that fibril growth involves the formation of an obligate intermediate, corresponding to a hairpin structure, which forms hydrogen bonds to the odd end of the fibril core. Identification of such an intermediate provides a tunable, druggable pivot in the folding pathway to fibril elongation and provides a checkpoint that can be exploited for basic research aiming to elucidate the mechanisms underlying the aggregation process.

■ ASSOCIATED CONTENT

Supporting Information

Figures S1−S10

. This material is available free of charge via the Internet at http://pubs.acs.org.

■ AUTHOR INFORMATION

Corresponding Author

*E-mail: cmstultz@mit.edu.

Funding

This material is based upon work supported, in part, by National Science Foundation Grant 0821391.

Notes

The authors declare no competing financial interest.

■ ACKNOWLEDGMENTS

We thank Linder Cândido da Silva for implementing the Gaussian-based function for strand content.

■ REFERENCES

(1) Zhang, S., Iwata, K., Lachenmann, M. J., Peng, J. W., Li, S., Stimson, E. R., Lu, Y. a., Felix, A. M., Maggio, J. E., and Lee, J. P. (2000) The Alzheimer's Peptide Aβ Adopts a Collapsed Coil Structure in Water. *J. Struct. Biol. 130*, 130−141.

(2) Hardy, J., and Selkoe, D. J. (2002) The Amyloid Hypothesis of Alzheimer's Disease: Progress and Problems on the Road to Therapeutics. *Science 297*, 353−356.

(3) Haass, C., and Selkoe, D. J. (2007) Soluble protein oligomers in neurodegeneration: Lessons from the Alzheimer's amyloid β-peptide. *Nat. Rev. Mol. Cell Biol. 8*, 101−112.

(4) Yan, Y., and Wang, C. (2006) Aβ42 is More Rigid than Aβ40 at the C Terminus: Implications for Aβ Aggregation and Toxicity. *J. Mol. Biol. 364*, 853−862.

(5) Roher, A. E., Lowenson, J. D., Clarke, S., Woods, A. S., Cotter, R. J., Gowing, E., and Ball, M. J. (1993) β-Amyloid-(1−42) is a major component of cerebrovascular amyloid deposits: Implications for the pathology of Alzheimer disease. *Proc. Natl. Acad. Sci. U.S.A. 90*, 10836−10840.

(6) El-Agnaf, O. M. A., Mahil, D. S., Patel, B. P., and Austen, B. M. (2000) Oligomerization and Toxicity of β-Amyloid-42 Implicated in Alzheimer's Disease. *Biochem. Biophys. Res. Commun. 273*, 1003−1007.

(7) Jarrett, J. T., Berger, E. P., and Lansbury, P. T. (1993) The C-Terminus of the β Protein is Critical in Amyloidogenesisa. *Ann. N.Y. Acad. Sci. 695*, 144−148.

(8) Walsh, D. M., Klyubin, I., Fadeeva, J. V., Cullen, W. K., Anwyl, R., Wolfe, M. S., Rowan, M. J., and Selkoe, D. J. (2002) Naturally secreted oligomers of amyloid β protein potently inhibit hippocampal long-term potentiation in vivo. *Nature 416*, 535−539.

(9) Cohen, S. I. A., Linse, S., Luheshi, L. M., Hellstrand, E., White, D. A., Rajah, L., Otzen, D. E., Vendruscolo, M., Dobson, C. M., and Knowles, T. P. J. (2013) Proliferation of amyloid-β42 aggregates occurs through a secondary nucleation mechanism. *Proc. Natl. Acad. Sci. U.S.A. 110*, 9758−9763.

(10) Schnabel, J. (2011) Amyloid: Little proteins, big clues. *Nature 475*, S12−S14.

(11) Bernstein, S. L., Dupuis, N. F., Lazo, N. D., Wyttenbach, T., Condron, M. M., Bitan, G., Teplow, D. B., Shea, J.-E., Ruotolo, B. T., Robinson, C. V., and Bowers, M. T. (2009) Amyloid-β protein oligomerization and the importance of tetramers and dodecamers in the aetiology of Alzheimer's disease. *Nat. Chem. 1*, 326−331.

(12) Lührs, T., Ritter, C., Adrian, M., Riek-Loher, D., Bohrmann, B., Döbeli, H., Schubert, D., and Riek, R. (2005) 3D structure of Alzheimer's amyloid-β(1−42) fibrils. *Proc. Natl. Acad. Sci. U.S.A. 102*, 17342−17347.

(13) Bernstein, F. C., Koetzle, T. F., Williams, G. J. B., Meyer, E. F., Jr., Brice, M. D., Rodgers, J. R., Kennard, O., Shimanouchi, T., and Tasumi, M. (1977) The protein data bank: A computer-based archival file for macromolecular structures. *J. Mol. Biol. 112*, 535−542.

(14) Petkova, A. T., Yau, W.-M., and Tycko, R. (2006) Experimental Constraints on Quaternary Structure in Alzheimer's β-Amyloid Fibrils. *Biochemistry 45*, 498−512.

(15) Brooks, B. R., Bruccoleri, R. E., Olafson, B. D., States, D. J., Swaminathan, S., and Karplus, M. (1983) CHARMM: A program for macromolecular energy, minimization, and dynamics calculations. *J. Comput. Chem. 4*, 187−217.

(16) Vitalis, A., Lyle, N., and Pappu, R. V. (2009) Thermodynamics of β-Sheet Formation in Polyglutamine. *Biophys. J. 97*, 303−311.

(17) Kabsch, W., and Sander, C. (1983) Dictionary of protein secondary structure: Pattern recognition of hydrogen-bonded and geometrical features. *Biopolymers 22*, 2577−2637.

(18) Brooks, B. R., Brooks, C. L., Mackerell, A. D., Nilsson, L., Petrella, R. J., Roux, B., Won, Y., Archontis, G., Bartels, C., Boresch, S., Caflisch, A., Caves, L., Cui, Q., Dinner, A. R., Feig, M., Fischer, S., Gao, J.,

Hodoscek, M., Im, W., Kuczera, K., Lazaridis, T., Ma, J., Ovchinnikov, V., Paci, E., Pastor, R. W., Post, C. B., Pu, J. Z., Schaefer, M., Tidor, B., Venable, R. M., Woodcock, H. L., Wu, X., Yang, W., York, D. M., and Karplus, M. (2009) CHARMM: The biomolecular simulation program. *J. Comput. Chem. 30*, 1545−1614.
(19) Dashti, D. S., and Roitberg, A. E. (2013) Optimization of Umbrella Sampling Replica Exchange Molecular Dynamics by Replica Positioning. *J. Chem. Theory Comput. 9*, 4692−4699.
(20) Wang, D. Q., Amundadottir, M. L., van Gunsteren, W. F., and Hunenberger, P. H. (2013) Intramolecular hydrogen-bonding in aqueous carbohydrates as a cause or consequence of conformational preferences: A molecular dynamics study of cellobiose stereoisomers. *Eur. Biophys. J. 42*, 521−537.
(21) Wilhelm, M., Mukherjee, A., Bouvier, B., Zakrzewska, K., Hynes, J. T., and Lavery, R. (2012) Multistep Drug Intercalation: Molecular Dynamics and Free Energy Studies of the Binding of Daunomycin to DNA. *J. Am. Chem. Soc. 134*, 8588−8596.
(22) Lazaridis, T., and Karplus, M. (1999) Effective energy function for proteins in solution. *Proteins: Struct., Funct., Bioinf. 35*, 133−152.
(23) Huang, A., and Stultz, C. M. (2007) Conformational sampling with implicit solvent models: Application to the PHF6 peptide in tau protein. *Biophys. J. 92*, 34−45.
(24) Strodel, B., and Wales, D. J. (2008) Implicit solvent models and the energy landscape for aggregation of the amyloidogenic KFFE peptide. *J. Chem. Theory Comput. 4*, 657−672.
(25) Evans, D. J., and Holian, B. L. (1985) The Nose-Hoover thermostat. *J. Chem. Phys. 83*, 4069−4074.
(26) Grossfield, A. (2013) *WHAM: The weighted histogram analysis method*, version 2.0.7, http://membrane.urmc.rochester.edu/content/wham.
(27) Kumar, S., Rosenberg, J. M., Bouzida, D., Swendsen, R. H., and Kollman, P. A. (1992) The weighted histogram analysis method for free-energy calculations on biomolecules. I. The method. *J. Comput. Chem. 13*, 1011−1021.
(28) Selkoe, D. J. (2003) Folding proteins in fatal ways. *Nature 426*, 900−904.
(29) Roux, B. (1995) The calculation of the potential of mean force using computer simulations. *Comput. Phys. Commun. 91*, 275−282.
(30) Ahmed, M., Davis, J., Aucoin, D., Sato, T., Ahuja, S., Aimoto, S., Elliott, J. I., Van Nostrand, W. E., and Smith, S. O. (2010) Structural conversion of neurotoxic amyloid-β1−42 oligomers to fibrils. *Nat. Struct. Mol. Biol. 17*, 561−567.
(31) Paravastu, A. K., Leapman, R. D., Yau, W.-M., and Tycko, R. (2008) Molecular structural basis for polymorphism in Alzheimer's β-amyloid fibrils. *Proc. Natl. Acad. Sci. U.S.A. 105*, 18349−18354.
(32) Fitzpatrick, A. W. P., Debelouchina, G. T., Bayro, M. J., Clare, D. K., Caporini, M. A., Bajaj, V. S., Jaroniec, C. P., Wang, L., Ladizhansky, V., Müller, S. A., MacPhee, C. E., Waudby, C. A., Mott, H. R., De Simone, A., Knowles, T. P. J., Saibil, H. R., Vendruscolo, M., Orlova, E. V., Griffin, R. G., and Dobson, C. M. (2013) Atomic structure and hierarchical assembly of a cross-β amyloid fibril. *Proc. Natl. Acad. Sci. U.S.A. 110*, 5468−5473.
(33) GhattyVenkataKrishna, P. K., Uberbacher, E. C., and Cheng, X. (2013) Effect of the amyloid β hairpin's structure on the handedness of helices formed by its aggregates. *FEBS Lett. 587*, 2649−2655.
(34) Rubin, N., Perugia, E., Goldschmidt, M., Fridkin, M., and Addadi, L. (2008) Chirality of Amyloid Suprastructures. *J. Am. Chem. Soc. 130*, 4602−4603.
(35) Hoyer, W., Grönwall, C., Jonsson, A., Ståhl, S., and Härd, T. (2008) Stabilization of a β-hairpin in monomeric Alzheimer's amyloid-β peptide inhibits amyloid formation. *Proc. Natl. Acad. Sci. U.S.A. 105*, 5099−5104.
(36) Sciarretta, K. L., Gordon, D. J., Petkova, A. T., Tycko, R., and Meredith, S. C. (2005) Aβ40-Lactam(D23/K28) Models a Conformation Highly Favorable for Nucleation of Amyloid. *Biochemistry 44*, 6003−6014.
(37) Reddy, G., Straub, J. E., and Thirumalai, D. (2009) Influence of Preformed Asp23−Lys28 Salt Bridge on the Conformational Fluctuations of Monomers and Dimers of Aβ Peptides with Implications for Rates of Fibril Formation. *J. Phys. Chem. B 113*, 1162−1172.
(38) Tarus, B., Straub, J. E., and Thirumalai, D. (2006) Dynamics of Asp23−Lys28 Salt-Bridge Formation in Aβ10−35 Monomers. *J. Am. Chem. Soc. 128*, 16159−16168.
(39) Fisher, C. K., Ullman, O., and Stultz, C. M. (2013) Comparative Studies of Disordered Proteins with Similar Sequences: Application to Aβ40 and Aβ42. *Biophys. J. 104*, 1546−1555.
(40) Nguyen, P. H., Li, M. S., Stock, G., Straub, J. E., and Thirumalai, D. (2007) Monomer adds to preformed structured oligomers of Aβ-peptides by a two-stage dock-lock mechanism. *Proc. Natl. Acad. Sci. U.S.A. 104*, 111−116.
(41) Takeda, T., and Klimov, D. K. (2009) Probing Energetics of Aβ Fibril Elongation by Molecular Dynamics Simulations. *Biophys. J. 96*, 4428−4437.
(42) Rojas, A., Liwo, A., Browne, D., and Scheraga, H. A. (2010) Mechanism of Fiber Assembly: Treatment of Aβ Peptide Aggregation with a Coarse-Grained United-Residue Force Field. *J. Mol. Biol. 404*, 537−552.
(43) Esler, W. P., Stimson, E. R., Jennings, J. M., Vinters, H. V., Ghilardi, J. R., Lee, J. P., Mantyh, P. W., and Maggio, J. E. (2000) Alzheimer's disease amyloid propagation by a template-dependent dock-lock mechanism. *Biochemistry 39*, 6288−6295.
(44) Elenewski, J. E., and Hackett, J. C. (2010) Free Energy Landscape of the Retinol/Serum Retinol Binding Protein Complex: A Biological Host-Guest System. *J. Phys. Chem. B 114*, 11315−11322.
(45) Zhang, D. Q., Gullingsrud, J., and McCammon, J. A. (2006) Potentials of mean force for acetylcholine unbinding from the α7 nicotinic acetylcholine receptor ligand-binding domain. *J. Am. Chem. Soc. 128*, 3019−3026.
(46) Rashid, M. H., and Kuyucak, S. (2014) Free Energy Simulations of Binding of HsTx1 Toxin to Kv1 Potassium Channels: The Basis of Kv1.3/Kv1.1 Selectivity. *J. Phys. Chem. B 118*, 707−716.
(47) Dinner, A. R., and Karplus, M. (1999) Is protein unfolding the reverse of protein folding? A lattice simulation analysis. *J. Mol. Biol. 292*, 403−419.
(48) Daggett, V. (2002) Molecular Dynamics Simulations of the Protein Unfolding/Folding Reaction. *Acc. Chem. Res. 35*, 422−429.
(49) Fawzi, N. L., Ying, J., Ghirlando, R., Torchia, D. A., and Clore, G. M. (2011) Atomic-resolution dynamics on the surface of amyloid-β protofibrils probed by solution NMR. *Nature 480*, 268−272.
(50) Kumar-Singh, S., Julliams, A., Nuydens, R., Ceuterick, C., Labeur, C., Serneels, S., Vennekens, K. L., Van Osta, P., Geerts, H., De Strooper, B., and Van Broeckhoven, C. (2002) In Vitro Studies of Flemish, Dutch, and Wild-Type β-Amyloid Provide Evidence for Two-Staged Neurotoxicity. *Neurobiol. Dis. 11*, 330−340.
(51) Nilsberth, C., Westlind-Danielsson, A., Eckman, C. B., Condron, M. M., Axelman, K., Forsell, C., Stenh, C., Luthman, J., Teplow, D. B., Younkin, S. G., Naslund, J., and Lannfelt, L. (2001) The 'Arctic' APP mutation (E693G) causes Alzheimer's disease by enhanced Aβ protofibril formation. *Nat. Neurosci. 4*, 887−893.
(52) Langer, F., Eisele, Y. S., Fritschi, S. K., Staufenbiel, M., Walker, L. C., and Jucker, M. (2011) Soluble Aβ seeds are potent inducers of cerebral β-amyloid deposition. *J. Neurosci. 31*, 14488−14495.
(53) Lu, J.-X., Qiang, W., Yau, W.-M., Schwieters, C. D., Meredith, S. C., and Tycko, R. (2013) Molecular Structure of β-Amyloid Fibrils in Alzheimer's Disease Brain Tissue. *Cell 154*, 1257−1268.